COMPUTATIONAL EME COMPLIANCE ASSESSMENT OF THE DIGITAL VEHICULAR REPEATER (DVR VHF), MODEL #DQPMDVR3000P, FCC ID LO6-DVRSVHF AND XTL5000 VHF MOBILE RADIO, MODEL #M20KSS9PW1AN AND #M20KTS9PW1AN

January 10, 2006

Giorgi Bit-Babik and Antonio Faraone
Motorola Corporate EME Research Lab, Plantation, Florida

Introduction

This report summarizes the computational [numerical modeling] analysis performed to document compliance of the DVR VHF 6 watt model DQPMDVR3000P interfaced with, and transmitting simultaneously with, either companion VHF Mobile Radio models M20KSS9PW1AN or M20KTS9PW1AN with transmit powers up to 57 watts and vehicle-mounted antennas with the Federal Communications Commission (FCC) guidelines for human exposure to radio frequency (RF) emissions. The DVR radio operates in the 136 - 174 MHz frequency band while the companion VHF mobile radios operate in the 147-174 MHz band.

This computational analysis supplements the measurements conducted to evaluate the FCC *maximum permissible exposure* (MPE) limits for this mobile device. All test conditions (7 in total) that did not conform with applicable MPE limits were analyzed to determine whether those conditions complied with the *specific absorption rate* (SAR) limits for general public exposure (1.6 W/kg averaged over 1 gram of tissue and 0.08 W/kg averaged over the whole body) set forth in FCC guidelines, which are based on the IEEE C95.1-1999 standard [1]. In total 12 independent simulations have been performed. Six simulations are addressing the exposure to VHF mobile radios with roof-mount quarter wavelength antennas, and another six are addressing the exposure of passenger to the DVR VHF with trunk-mount quarter wavelength antennas. For both simulations groups, a commercial code based on Finite-Difference-Time-Domain (FDTD) methodology was employed to carry out the computational analysis. It is well established and recognized within the scientific community that SAR is the primary dosimetric quantity used to evaluate the human body's absorption of RF energy and that MPEs are in

fact derived from SAR. Accordingly, the SAR computations provide a scientifically valid and more relevant estimate of human exposure to RF energy.

Method

The simulation code employed is XFDTD™ v6.1, by Remcom Inc., State College, PA. This computational suite features a heterogeneous full body standing model (High Fidelity Body Mesh), derived from the so-called Visible Human [2], discretized in 5 mm voxels. The dielectric properties of 23 body tissues are automatically assigned by XFDTD™ at any specific frequency. The "seated" man model was obtained from the standing model by modifying the articulation angles at the hips and the knees. Details of the computational method and model are provided in the Appendix to this report, following the structure outlined in Appendix B.III of the Supplement C to the FCC OET Bulletin 65.

The car model has been imported into XFDTD™ from the CAD file of a sedan car having dimensions 4.98 m (L) x 1.85 m (W) x 1.18 m (H), and discretized in 5mm voxels. For the car model the wheels and part of the hood were omitted in order to fit within the computational memory available. These omissions would not be expected to affect the exposure calculations in any event.

For passenger exposure from VHF mobile radio roof-mount antennas the antenna was located in the center of the roof, so as to replicate the experimental conditions used in MPE measurements. Figures 1 shows one of the XFDTD™ computational models used for passenger exposure from the roof mounted antenna. For passenger exposure from DVR VHF trunk-mount antennas the distance of antennas from the passenger head was set at 85 cm and the antenna was located at 26 cm distance from the end of the trunk, so as to replicate the experimental conditions used in MPE measurements. Figures 2 shows one of the XFDTD™ computational models used for passenger exposure to trunk mounted antenna.

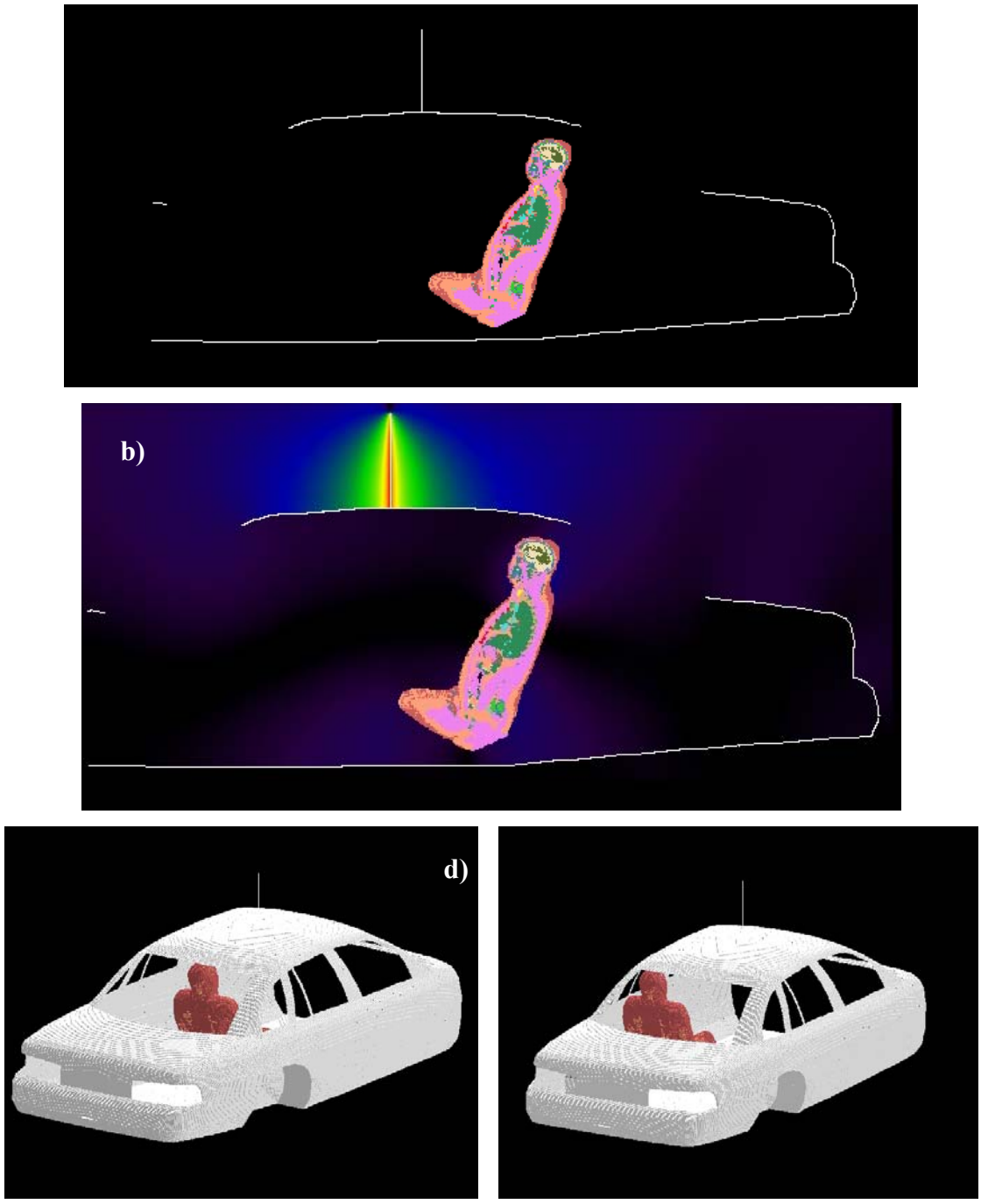

Figure 1: Passenger model exposed to a roof-mount antenna (43 cm) operating at 174 MHz: XFDTD geometry (a) and H-field distribution (b). The antenna is mounted in the center of the roof. The passenger model is located either in the center (c) or on the side of the back seat (d).

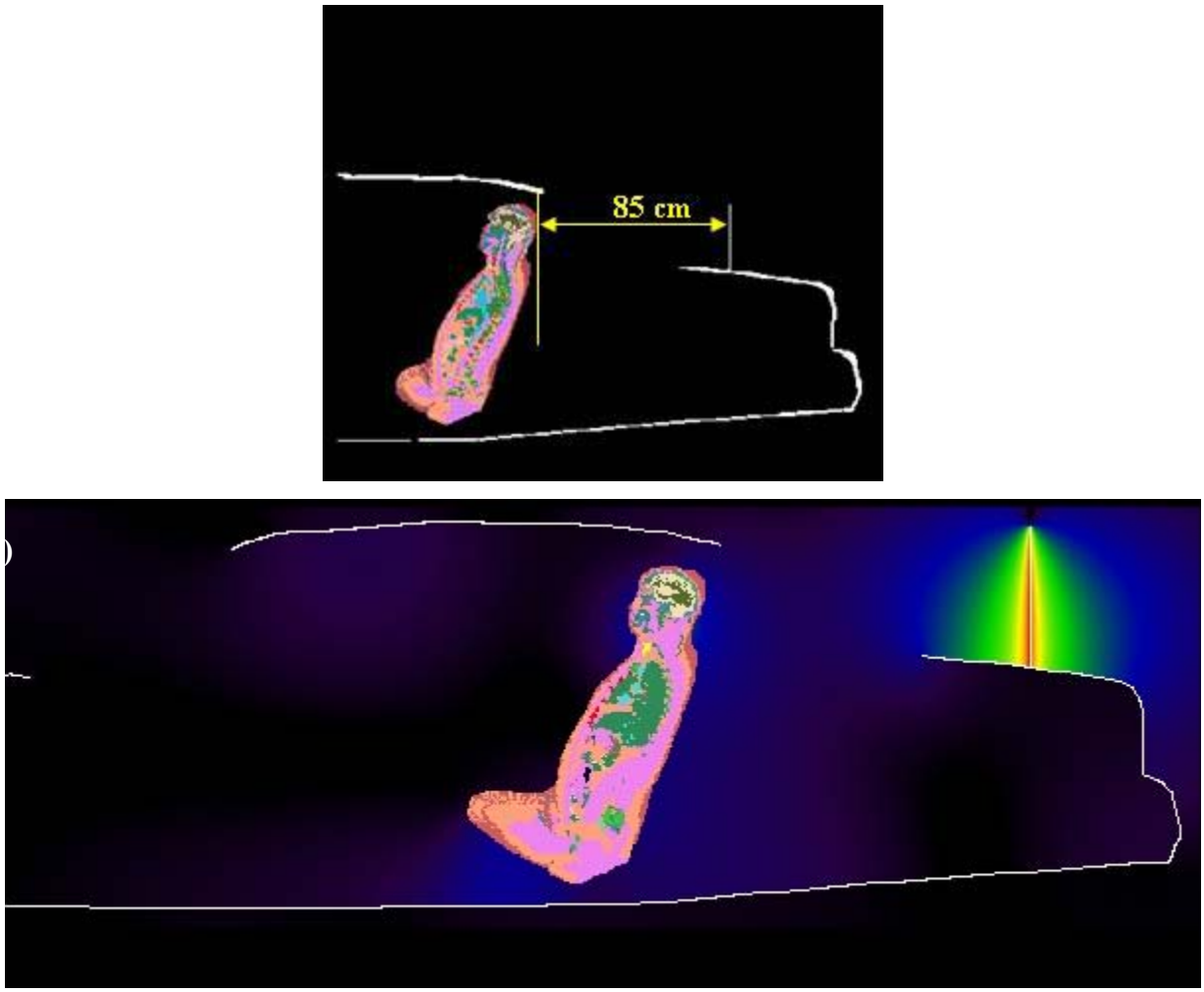

Figure 2: Passenger model exposed to a trunk-mount antenna (43 cm) operating at 174 MHz: XFDTD geometry (a) and H-field distribution (b). The antenna is mounted at 85 cm from the passenger.

The computational code employs a time-harmonic excitation to produce a steady state electromagnetic field in the exposed body. Subsequently, the corresponding SAR distribution is automatically processed in order to determine the whole-body and 1-g average SAR. The maximum output power from VHF mobile radio antenna is 57 W *rms*. Since the ohmic losses in the cable and in the car materials, as well as the mismatch losses at the antenna feed-point, are neglected, and source-based time averaging (50% talk time) is employed, all computational results are normalized to half of it, i.e., 28.5 W *rms* net output power. The maximum output power from DVR VHF system is 6 W *rms* and the computational results are normalized to 6 W *rms*. Two independent set simulations, one for DVR VHF trunk mount antenna and one for VHF radio roof-mount antenna were performed. Since VHF mobile radio and DVR VHF repeater can transmit simultaneously, the maximum peak and whole body average SAR results from

each set of data were combined for the corresponding passenger location to produce peak SAR value for the composite exposure from both roof and trunk-mount antennas. The obtained composite peak SAR value is an overestimation of the actual exposure because the peak SAR values from the roof- and trunk-mount antennas that contribute to the composite value are not found at the same location in the body.

Results of SAR computations for car passengers

The test conditions for DVR VHF repeater requiring SAR computations are summarized in Table I, together with the antenna data and the SAR results. The conditions are for antenna mounted on the trunk. The passenger is located in the center or on the side of the rear seat. The passenger model is surrounded by air, as the seat, which is made out of poorly conductive fabrics, is not included in the computational model. All the transmit frequency, antenna length, and passenger location combinations reported in Table I have been simulated individually.

Table I: Results of the SAR computations for passenger exposure from DVR VHF trunk-mount antennas

MPE Table #	Mount location	Antenna Kit #	Antenna length		Freq [MHz]	Exposure location	SAR [W/kg]	
			Physical	XFDTD			1-g	WB
1	Trunk	**HAD4006A**	52.0 cm	52.0 cm	136	center	0.070	0.0020
2	Trunk	**HAD4008A**	45.6 cm	45.5 cm	155	center	0.12	0.0053
3	Trunk	**HAD4009A**	43.0 cm	43.0 cm	174	center	0.10	0.0047
4	Trunk	**HAD4006A**	52.0 cm	52.0 cm	136	side	0.048	0.0032
5	Trunk	**HAD4008A**	45.6 cm	45.5 cm	155	side	0.050	0.0033
6	Trunk	**HAD4009A**	43.0 cm	43.0 cm	174	side	0.048	0.0026

The test conditions for VHF mobile radio requiring SAR computations are summarized in Table II, together with the antenna data and the SAR results. The conditions are for antenna mounted on the roof. The passenger is located at the same location as in previously described conditions, i.e. in the center or on the side of the rear seat. All the transmit frequency, antenna length, and passenger location combinations reported in Table II have been simulated individually.

Table II: Results of the SAR computations for passenger exposure from VHF mobile radio roof-mount antennas (50% talk time)

MPE Table #	Mount location	Antenna Kit #	Antenna length		Freq [MHz]	Exposure location	SAR [W/kg]	
			Physical	XFDTD			1-g	WB
1	Roof	**HAD4007A**	49.0 cm	49.0 cm	147	center	0.15	0.0069
2	Roof	**HAD4008A**	45.6 cm	45.5 cm	155	center	0.078	0.0050
3	Roof	**HAD4009A**	43.0 cm	43.0 cm	174	center	0.11	0.0067
4	Roof	**HAD4007A**	49.0 cm	49.0 cm	147	side	0.099	0.0061
5	Roof	**HAD4008A**	45.6 cm	45.5 cm	155	side	0.097	0.0061
6	Roof	**HAD4009A**	43.0 cm	43.0 cm	174	side	0.18	0.0083

For each location of the passenger on the back seat (center and side) the peak SAR values were identified for both DVR VHF and VHF mobile radio exposure and then combined to produce the composite peak SAR value. Table III and Table IV present those values.

Table III: Peak 1-g average SAR for both passenger locations on the back seat and composite 1-g average SAR from simultaneous exposure.

Passenger location	DVR VHF [W/kg]	VHF mobile radio [W/kg]	Total SAR [W/kg]
Center of the back seat	0.12	0.15	0.27
Side of the back seat	0.05	0.18	0.23

Table IV: Peak whole body average SAR for both passenger locations on the back seat and composite whole body average SAR from simultaneous exposure.

Passenger location	DVR VHF [W/kg]	VHF mobile radio [W/kg]	Total SAR [W/kg]
Center of the back seat	0.0053	0.0069	0.0122
Side of the back seat	0.0033	0.0083	0.0116

From Table III and Table IV the maximum combined peak 1-g SAR is 0.27 W/kg which occurs in the body located in the center of the back seat, while the maximum combined whole-body average SAR is 0.012 W/kg which occurs in the body located on the side of the back seat.

The SAR distribution in the passenger model in the exposure condition with DVR VHF radio trunk-mount antennas that gave highest 1-g SAR is reported in Fig. 3 (155 MHz, passenger in the center of the back seat, HAD4008A antenna). The same condition produced highest whole body average SAR.

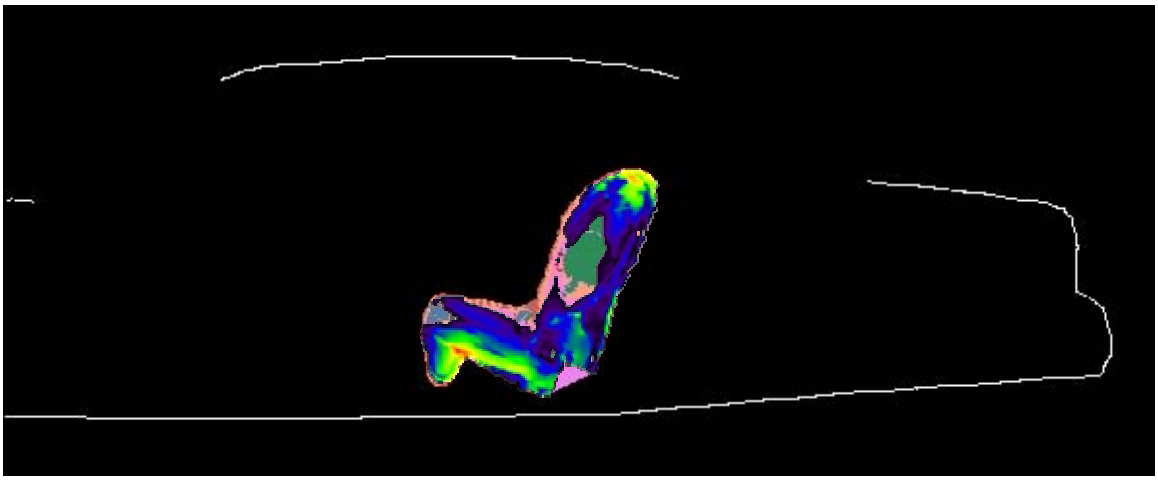

Figure 3. SAR and field distribution at 155 MHz in the passenger located in the center of the back seat, produced by the trunk-mount HAD4008A antenna. The contour plot in the figure is relative to the plane where the peak 1-g average SAR for this exposure condition occurs.

The SAR distribution in the passenger model in the exposure condition with VHF mobile radio roof-mount antennas that gave highest 1-g SAR is reported in Fig. 4 (174 MHz, passenger in the side of the back seat, HAD4009A antenna). The same condition produced highest whole body average SAR.

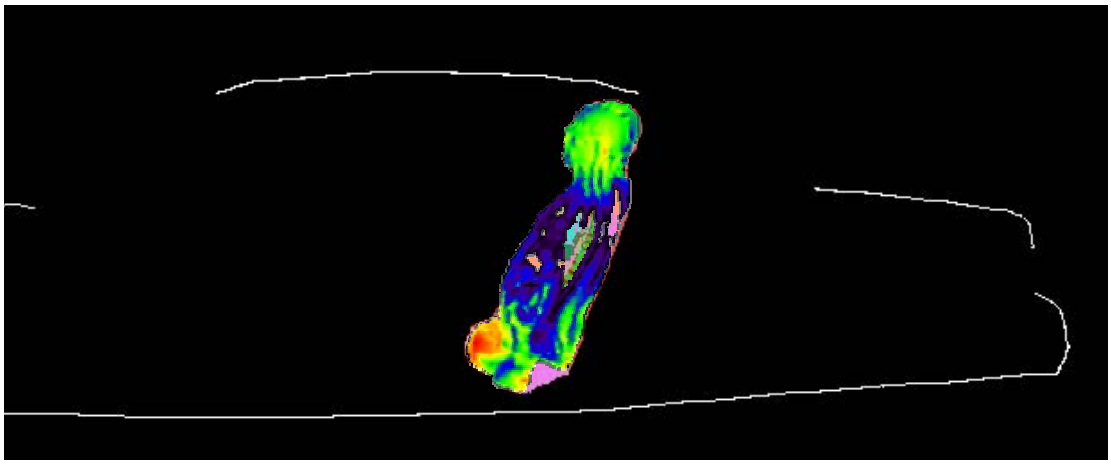

Figure 4. SAR distribution at 174 MHz in the passenger located on the side of the back seat, produced by the roof-mount HAD4009A antenna. The contour plot in the figure is relative to the plane where the peak 1-g average SAR for this exposure condition occurs.

Conclusions

Under the test conditions described for evaluating passenger and bystander exposure to the RF electromagnetic fields emitted by vehicle-mounted antennas used in conjunction with this mobile radio product, the present analysis shows that the computed SAR values are compliant with the FCC exposure limits for the general public.

References

[1] IEEE Standard C95.1-1999. *IEEE Standard for Safety Levels with Respect to Human Exposure to RF Electromagnetic Fields*, 3 kHz to 300 GHz.

[2] http://www.nlm.nih.gov/research/visible/visible_human.html

APPENDIX: SPECIFIC INFORMATION FOR SAR COMPUTATIONS

This appendix follows the structure outlined in Appendix B.III of the Supplement C to the FCC OET Bulletin 65. Most of the information regarding the code employed to perform the numerical computations has been adapted from the XFDTD™ v5.3 User Manual. Remcom Inc., owner of XFDTD™, is kindly acknowledged for the help provided.

1) Computational resources

a) A distributed Linux based multi-CPU computer cluster (Altrix) equipped with 64-bit Intel processors was employed for all simulations.

b) The memory requirement was close to 3 GB in all cases. Using the above-mentioned system with four processors operating concurrently, the typical simulation would run for 10 hours.

2) FDTD algorithm implementation and validation

a) We employed a commercial code (XFDTD™ v5.3, by Remcom Inc.) that implements the classical Yee's FDTD formulation [1]. The solution domain was discretized according to a rectangular grid with a uniform 5 mm step in all directions. Sub-gridding was not used. Liao's absorbing boundary conditions [2] are set at the domain boundary to simulate free space radiation processes. The excitation is a lumped voltage generator with 50-ohm source impedance. The code allows selecting *wire objects* without specifying their radius. We used a wire to represent the antenna. The car body is modeled by solid metal. We did not employ the "thin wire" algorithm in XFDTD™ since the antenna radius was never smaller than one-fifth the voxel dimension. In fact, the XFDTD™ manual specifies that "Thin Wire materials may be used in special situations where a wire with a radius much smaller than the cell size is required… in cases where the wire radius is important to the calculation and is less than approximately 1/5 the cell size, the thin wire material may be used to accurately simulate the correct wire dimensions." The voxel size in all our simulations was 5 mm, and the antenna radius is always at least 1 mm (1 mm for the short quarter-wave antennas and 1.5 mm for the long gain antennas), so there was no need to specify a "thin wire" material. Because the field impinges on the bystander or passenger model at a distance of several tens of voxels from the antenna, the details of antenna wire modeling are not expected to have significant impact on the exposure level.

b) XFDTD™ is one of the most widely employed commercial codes for electromagnetic simulations. It has gone through extensive validation and has proven its accuracy over time in many different applications. One example is provided in [3].

We carried out a validation of the code algorithm by running the canonical test case involving a half-wave wire dipole. The dipole is 0.475 times the free space wavelength at 160 MHz, i.e., 88.5 cm long. The discretization used in the model was uniform in all directions and equal to 5 mm, so the dipole was 177 cells long. Also in this case, the "thin wire" model was not needed. The following picture shows XFDTD™ outputs regarding the antenna feed-point impedance (72.5 – j 11.8 ohm), as well as qualitative distributions of the total E and H fields near the dipole. The radiation pattern is shown as well (one lobe in elevation). As expected, the 3 dB beamwidth is about 78 degrees.

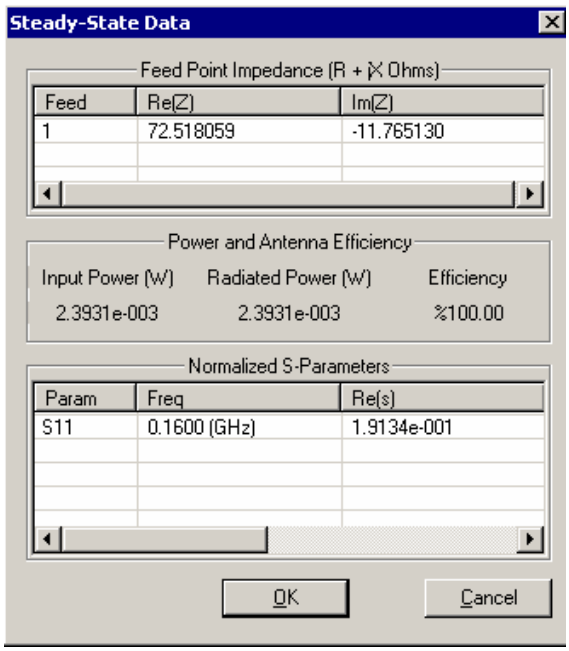

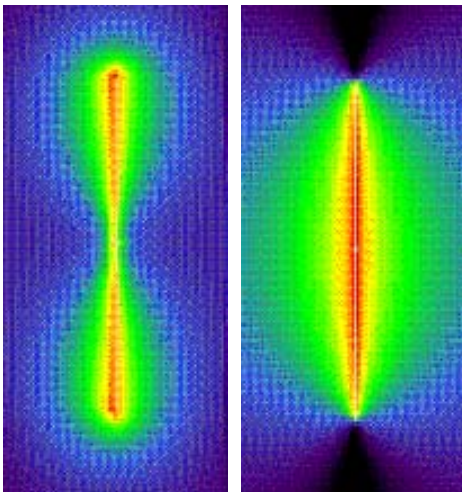

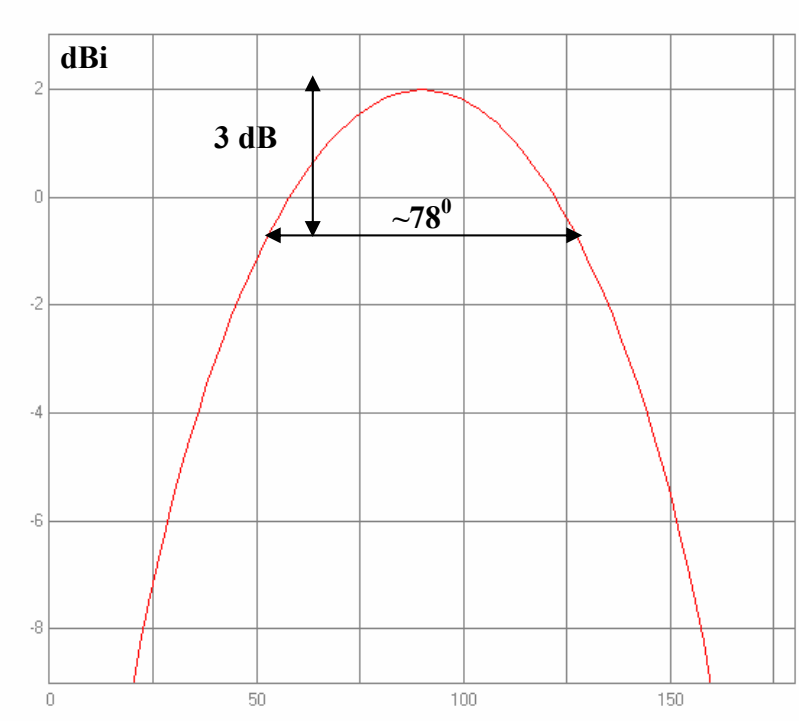

Elevation Angle [degrees]

We also compared the XFDTD™ result with the results derived from NEC [4], which is a code based on the method of moments. In this case, we used a dipole with radius 1 mm, length 88.5 cm, and the discretization is 5 mm. The corresponding input impedance at 160 MHz is 69.5-j10.5 ohm. Its frequency dependence is reported in the following figure.

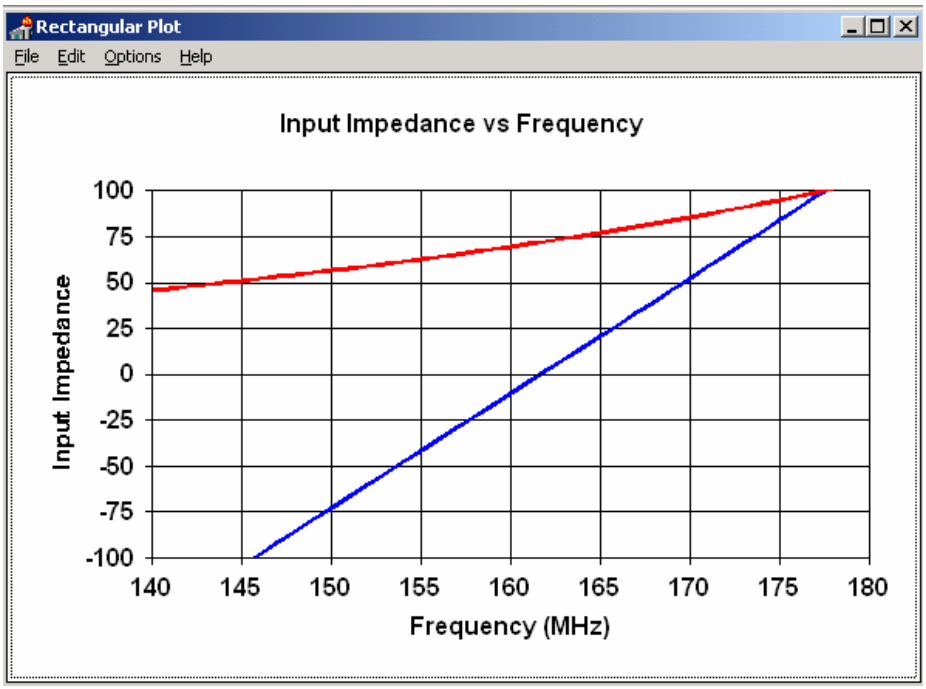

This validation ensures that the input impedance calculation is carried out correctly in XFDTD™, thereby enabling accurate estimates of the radiated power. It further ensures that the wire model employed in XFDTD™, which we used to model the antennas, produces physically meaningful current and fields distributions. Both these aspects ensure that the field quantities are correctly computed both in terms of absolute amplitude and relative distribution.

3) Computational parameters

a) The following table reports the main parameters of the FDTD model employed to perform our computational analysis:

PARAMETER	X	Y	Z
Voxel size	5 mm	5 mm	5 mm
Maximum domain dimensions employed for passenger computations with the roof-mount antennas	387	737	342
Maximum domain dimensions employed for passenger computations with the trunk-mount antennas	387	737	256
Time step	Exactly equal to Courant limit (typically 10 *ps* at this frequency, with the body model)		
Objects separation from FDTD boundary (voxels)	>10	>10	>10
Number of time steps for passenger	At least 6000 in all simulations		
Excitation	Sinusoidal (approx. 9-10 periods)		

b) In order to fit the model within a grid size that would not use up the available memory, we chopped the hood of the car and the feet of the human model.

4) Phantom model implementation and validation

a) The FDTD mesh of a male human body was created using digitized data in the form of transverse color images. The data is from the *visible human project* sponsored by the National Library of Medicine (NLM) and is available via the Internet (http://www.nlm.nih.gov/research/visible/visible_human.html). The male data set consists of MRI, CT and anatomical images. Axial MRI images of the head and neck and longitudinal sections of the rest of the body are available at 4 mm intervals. The MRI images have 256 pixel by 256 pixel resolution. Each pixel has 12 bits of gray tone resolution. The CT data consists of axial CT scans of the entire body taken at 1 mm intervals at a resolution of 512 pixels by 512 pixels where each pixel is made up of 12 bits of gray tone. The axial anatomical images are 2048 pixels by 1216 pixels where each pixel is defined by 24 bits of color. The anatomical cross sections are also at 1 mm intervals and coincide with the CT axial images. There are 1871 cross sections. The XFDTD™ High Fidelity Body Mesh uses 5x5x5 mm cells and has dimensions 136 x 87 x 397. Dr. Michael Smith and Dr. Chris Collins of the Milton S. Hershey Medical Center, Hershey, Pa, created the High Fidelity Body mesh. Details of body model creation are given in the *methods* section in [5]. The body mesh contains 23 tissues materials. Measured values for the tissue parameters for a broad frequency range are included with the mesh data. The correct values are interpolated from the table of measured data and entered into the appropriate mesh variables. The tissue conductivity and permittivity variation *vs.* frequency is included in the XFDTD™ calculation by a multiple-pole approximation to the Cole-Cole approximated tissue parameters reported by Camelia Gabriel, Ph.D., and Sami Gabriel, M. Sc. (http://www.brooks.af.mil/AFRL/HED/hedr/reports/dielectric/home.html).

a) The XFDTD™ High Fidelity Body Mesh model correctly represents the anatomical structure and the dielectric properties of body tissues, so it is appropriate for determining the highest exposure expected for normal device operation.

b) One example of the accuracy of XFDTD™ for computing SAR has been provided in [6]. The study reported in [6] is relative to a large-scale benchmark of measurement and computational tools carried out within the IEEE Standards Coordinating Committee 34, Sub-Committee 2.

5) Tissue dielectric parameters

a) The following table reports the dielectric properties used by XFDTD™ for the 23 body tissue materials in the High Fidelity Body Mesh at 155 MHz (mid-band for this VHF mobile radio product).

#	Tissue	ε_r	σ (S/m)	Density (kg/m^3)
1	skin	50.5	0.49	1125
2	tendon, pancreas, prostate, aorta, liver, other	59.3	0.63	1151
3	fat, yellow marrow	5.8	0.04	943
4	cortical bone	15.5	0.08	1850
5	cancellous bone	26.0	0.17	1080
6	blood	64.5	1.65	1057
7	muscle, heart, spleen, colon, tongue	73.6	0.84	1059
8	gray matter, cerebellum	71.5	0.73	1035.5
9	white matter	51.4	0.41	1027.4
10	CSF	73.9	2.29	1000
11	sclera/cornea	61.8	0.94	1151
12	vitreous humor	68.6	1.52	1000
13	bladder	19.1	0.28	1132
14	nerve	44.0	0.41	1112
15	cartilage	53.8	0.53	1171
16	gall bladder bile	86.6	1.49	928
17	thyroid	65.9	0.71	1035.5
18	stomach/esophagus	78.5	1.03	1126
19	lung	52.3	0.59	563
20	kidney	72.9	1.02	1147
21	testis	72.6	0.99	1158
22	lens	57.3	0.61	1163
23	small intestine	89.5	1.85	1153

b) The tissue types and dielectric parameters used in the SAR computation are appropriate for determining the highest exposure expected for normal device operation, because they are derived from measurements performed on real biological tissues (http://www.brooks.af.mil/AFRL/HED/hedr/reports/dielectric/home.html).

c) The tabulated list of the dielectric parameters used in phantom models is provided at point 5(a). As regards the device (car plus antenna), we used perfect electric conductors.

6) Transmitter model implementation and validation

a) The essential features that must be modeled correctly for the particular test device model to be valid are:

- Car body. We developed one very similar to the car used for MPE measurements, so as to be able to correlate measured and simulated field values. The model was imported in XFDTD™ from a CAD model that is commercially available at http://www.3dcadbrowser.com/
- Antenna. We used a straight wire in all cases, even though the gain antenna has a base coil for tuning. All the coil does is compensating for excess capacitance due to the antenna being slightly longer than half a wavelength. We do not need to do that in the model, as we used normalization with respect to the net radiated power, which is determined by the input resistance only. In this way, we neglect mismatch losses and artificially produce an overestimation of the SAR, thereby introducing a conservative bias in the model.

- Antenna location. We used the same location, relative to the edge of the car trunk, the backseat, or the roof, used in the MPE measurements. The following pictures show a lateral and a perspective view of the whole model (XFDTD™ does not show wires in this type of view, that is why the antenna is not visible).

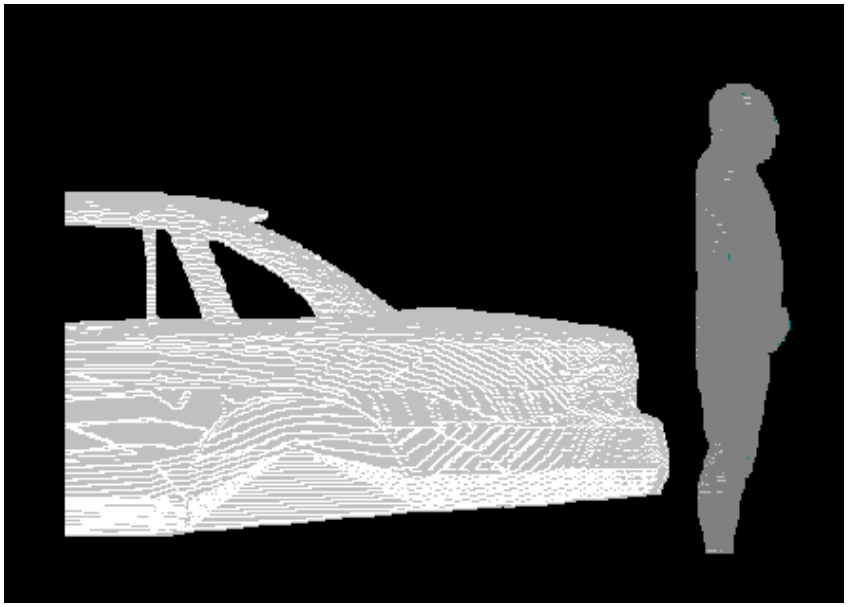

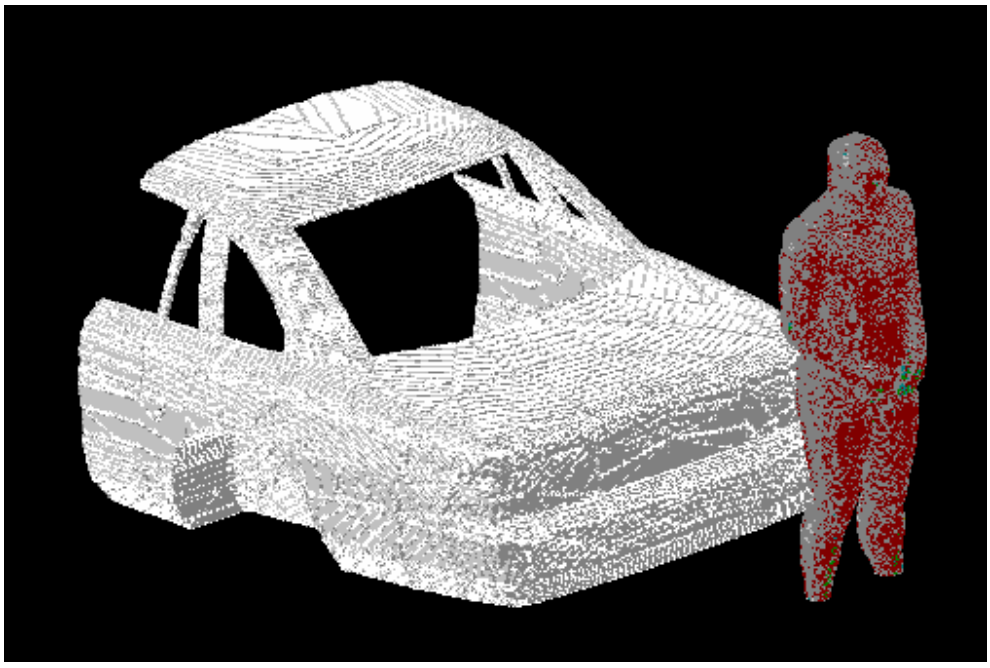

The car model is constituted by perfect electric conductor and does not include wheels in order to reduce its complexity. The passenger model is surrounded by air, as the seat, which is made out of poorly conductive fabrics, is not included in the computational model. The pavement has not been included in the model. The passenger and bystander models were validated for similar antenna and frequency conditions by comparing the MPE measurements at two VHF frequencies (146 MHz and 164 MHz) for antennas used for a VHF mobile radio analyzed previously in 2003 (FCC ID#ABZ99FT3046). The corresponding MPE measurements are reported in the compliance report relative to FCC ID#ABZ99FT3046. The comparison results are presented below, according to following definitions for

the equivalent power densities (based on E or H-field):

$$S_E = \frac{|\mathbf{E}|^2}{2\eta}, \quad S_H = \frac{\eta}{2}|\mathbf{H}|^2, \quad \eta = 377\ \Omega$$

Passenger with 43 cm monopole antenna (HAD4009A 164 MHz)

The following figures of the test model show the empty car model, where the yellow dotted line represents the back seat, as it can be observed from the right-hand side figure showing the passenger. The comparison has been performed by taking the computed steady-state field values at the locations corresponding to the head, chest, and legs along the yellow line and comparing them with the corresponding measurements. Such a comparison is carried out at the same rms power level (56.5 W) used in the measurements. Steady-state E-field and H-field distributions at a vertical plane transverse to the car and crossing the passenger's head are displayed as well. Finally, a picture of the antenna is shown.

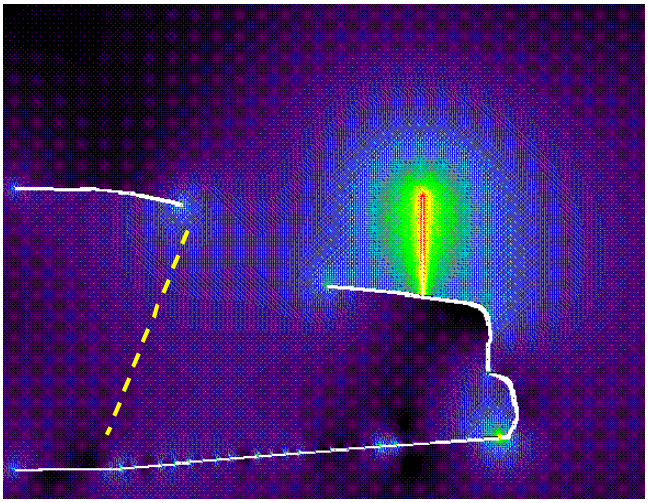

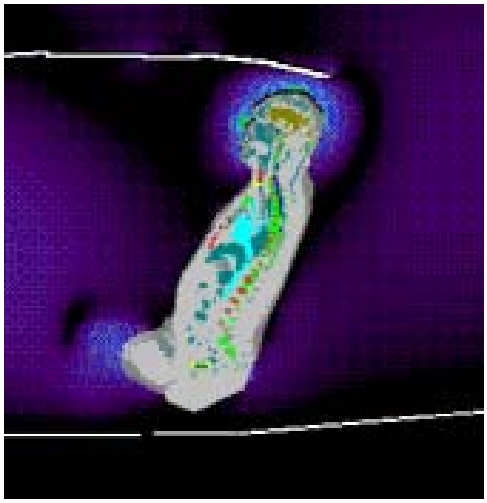

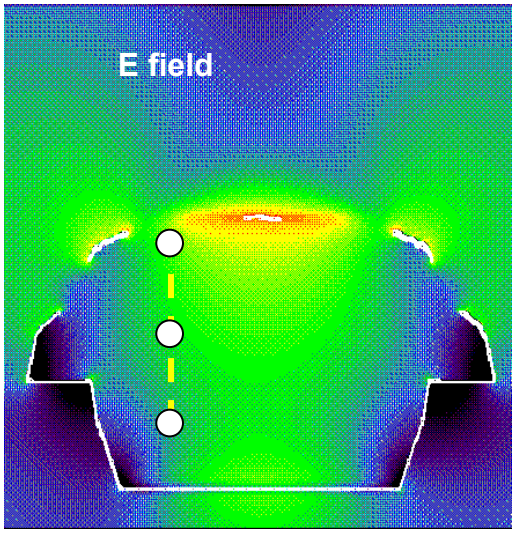

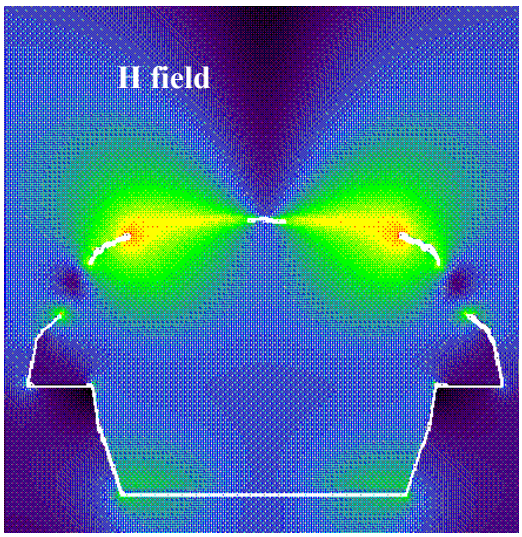

The highest exposure occurs in the middle of the backseat, which is also the case in the measurements. Therefore, the field values were determined on the yellow line centered at the middle of the backseat,

approximately at the three locations that are shown by white dots. In actuality, the line is inclined so as to follow the inclination of the passenger's back, as shown previously.

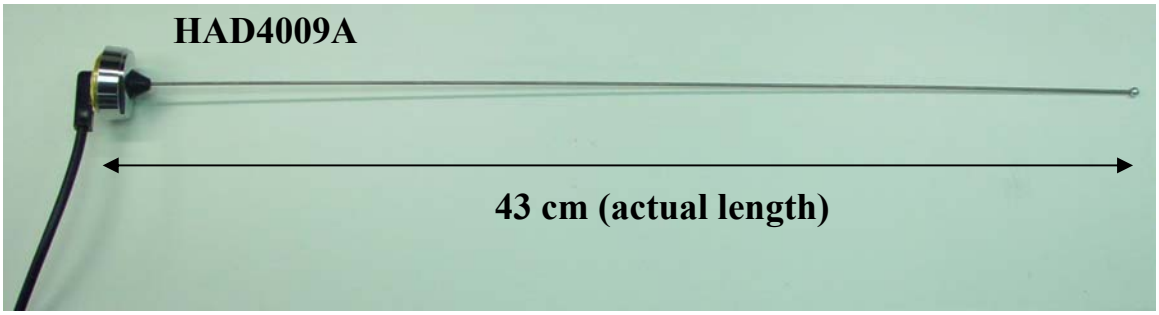

Because the peak exposure occurs in the center of the back seat, that was where we placed the passenger model to perform the SAR evaluations presented in the report. However, it can be observed that the H-field distribution features peaks near the lateral edges of the rear window. That is the reason why we also carried out one SAR computation by placing the passenger laterally in the back seat, in order to determine whether the SAR would be higher in this case.

As done in the measurements, the equivalent power density (S) is computed from the E-field, the H-field being much lower. The following table reports the E-field values computed by XFDTD™ at the three locations, and the corresponding power density.

Location	E-field magnitude (V/m)	S (W/m^2)
Head	1.0	1.33E-03
Chest	0.45	2.69E-04
Lower Trunk area	0.32	1.36E-04
	Average S	**5.77E-04**

The input impedance is 28.2-j27 ohm, therefore the radiated power (considering the mismatch to the 50 ohm unitary voltage source) is 2.06E-3 W. The scaled-up power density for 56.5 W radiated power is 15.8 W/m^2, corresponding to 1.58 mW/cm^2. Measurements gave an average of 1.29 mW/cm^2, which is in good agreement. The following table and the graph show a comparison between the simulated power density and the measured one (see also MPE report in FCC ID#ABZ99FT3046, Table 43), normalized to 56.5 W radiated.

Position	SE (meas) mW/cm^2	SE (FDTD) mW/cm^2
Head	2.98	3.64
Chest	0.74	0.74
Lower Trunk	0.14	0.37

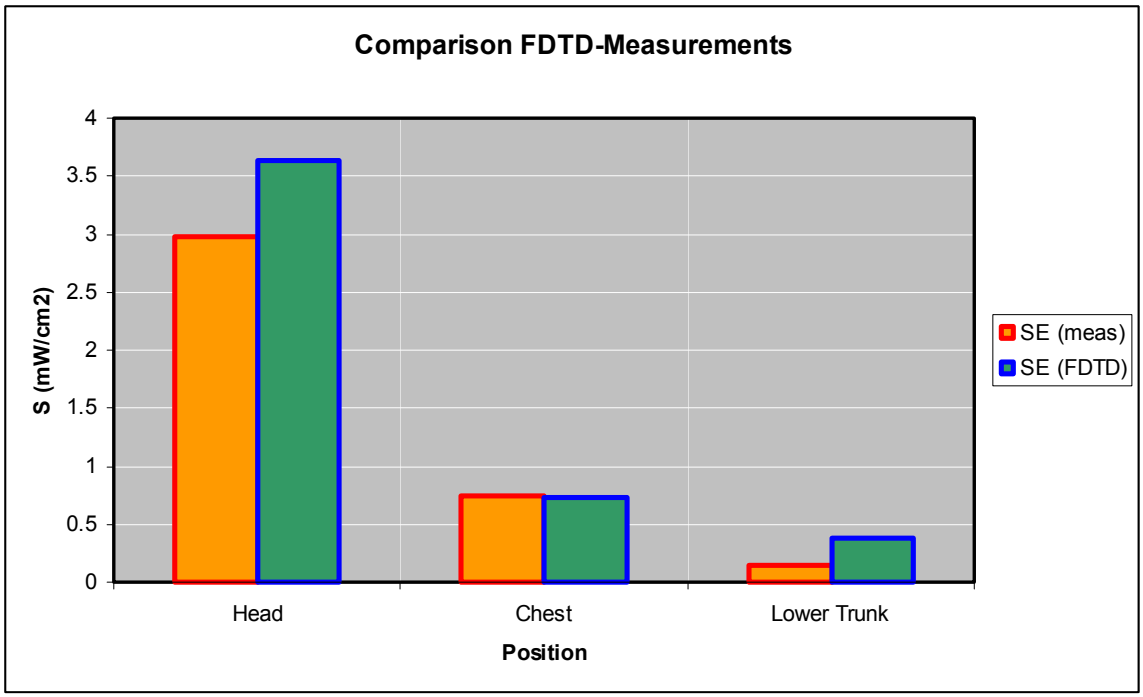

Bystander with 48 cm monopole antenna (HAD4007A 146 MHz)

The following figures show the E-field and H-field distributions across a vertical plane passing for the antenna and cutting the car in half. As done in the measurements, the MPE is computed from both E-field and H-field distributions, along the yellow dotted line at 10 points spaced 20 cm apart from each other up to 2 m in height. These lines and the field evaluation points are approximately indicated in the figures. The E-field and H-field distributions in the vertical plane placed at 60 cm from the antenna, behind the case, are shown as well. The points where the fields are sampled to determine the equivalent power density (S) are approximately indicated by the white dots. A picture of the antenna is not reported because it is identical to the HAD4009A except for the length.

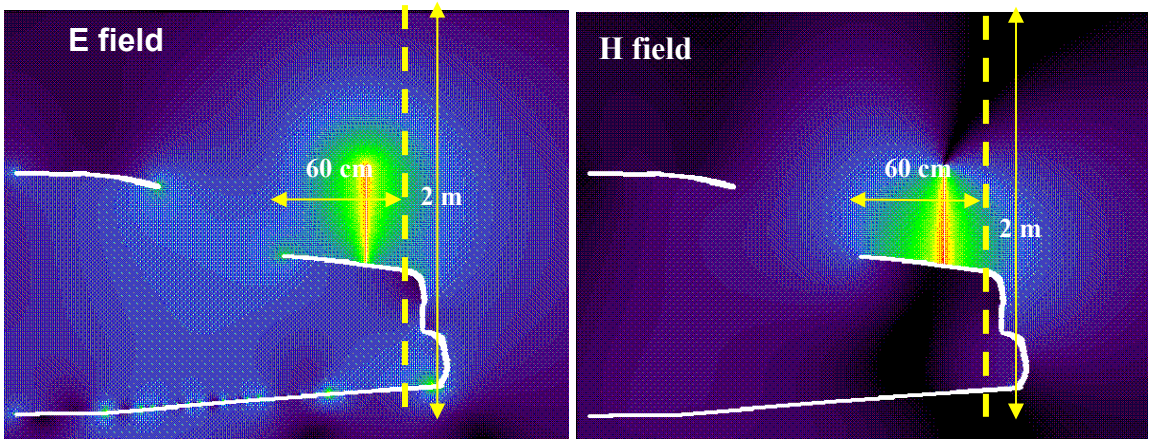

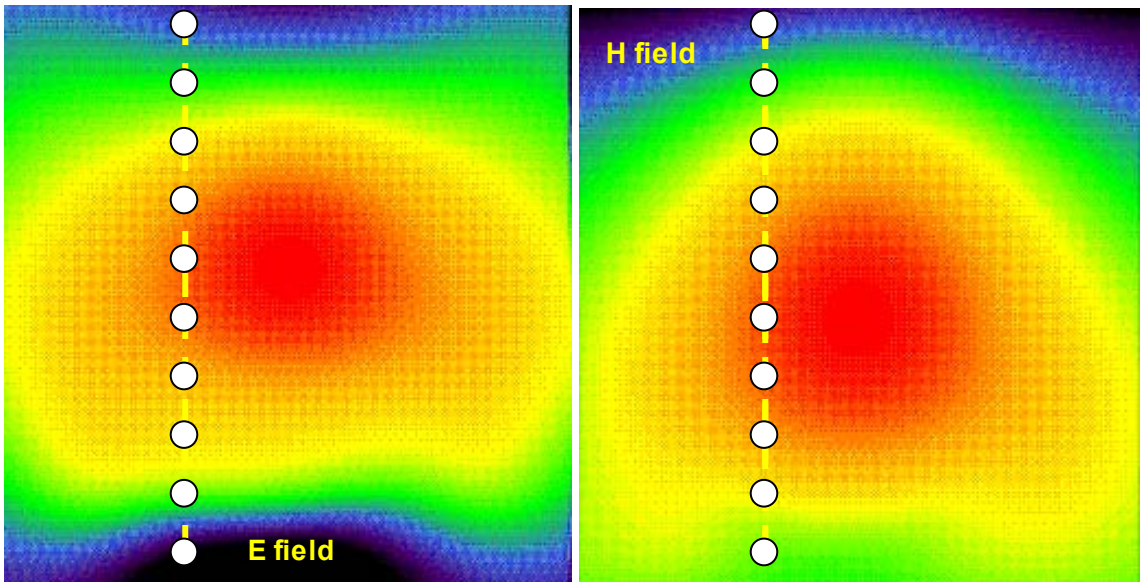

The following table reports the field values computed by XFDTD™ and the corresponding power density values. The average exposure levels are computed as well.

Height (cm)	E (V/m)	S_E (W/m^2)	H (A/m)	S_H (W/m^2)
20	2.12E-01	5.96E-05	5.14E-04	4.98E-05
40	3.81E-01	1.93E-04	8.67E-04	1.42E-04
60	4.43E-01	2.60E-04	1.35E-03	3.45E-04
80	5.36E-01	3.81E-04	1.73E-03	5.67E-04
100	6.17E-01	5.05E-04	1.84E-03	6.37E-04
120	6.28E-01	5.23E-04	1.57E-03	4.63E-04
140	5.59E-01	4.14E-04	1.11E-03	2.34E-04
160	4.41E-01	2.58E-04	6.99E-04	9.20E-05
180	3.24E-01	1.39E-04	3.73E-04	2.63E-05
200	2.31E-01	7.08E-05	1.86E-04	6.54E-06
	Average S_E	**2.80E-04**	**Average S_H**	**2.56E-04**

The input impedance is 27.3-j19.5 ohm, therefore the radiated power (considering the mismatch to the 50 ohm unitary voltage source) is 2.15E-3 W. The scaled-up power density values for 53.2 W radiated power are 6.93 W/m^2 (E), and 6.533 W/m^2 (H), that correspond to 0.69 mW/cm^2 (E), and 0.63 mW/cm^2 (H). Measurements yielded average power density of 0.664 mW/cm^2 (E), and 0.471 mW/cm^2 (H), i.e., which are in good agreement with the simulations. The following table and graph show a comparison between the simulated power density and the measured one, based on E (see MPE report in FCC ID#ABZ99FT3046, Table 1) or H fields (see MPE report in FCC ID#ABZ99FT3046, Table 13), normalized to 53.2 W radiated.

Height (cm)	SE (meas) mW/cm 2	SE (FDTD) mW/cm 2	SH (meas) mW/cm 2	SH (FDTD) mW/cm 2	Avg SE meas mW/cm 2	Avg SE FDTD mW/cm 2	Avg SH meas mW/cm 2	Avg SH FDTD mW/cm 2
20	0.19	0.15	0.2	0.12	0.664	0.694	0.471	0.634
40	0.37	0.48	0.23	0.35				
60	0.55	0.64	0.3	0.85				
80	0.68	0.94	0.56	1.40				
100	1.02	1.25	1.07	1.58				
120	1.15	1.29	1.1	1.15				
140	1.04	1.03	0.56	0.58				
160	0.79	0.64	0.24	0.23				
180	0.5	0.34	0.23	0.06				
200	0.35	0.18	0.22	0.02				

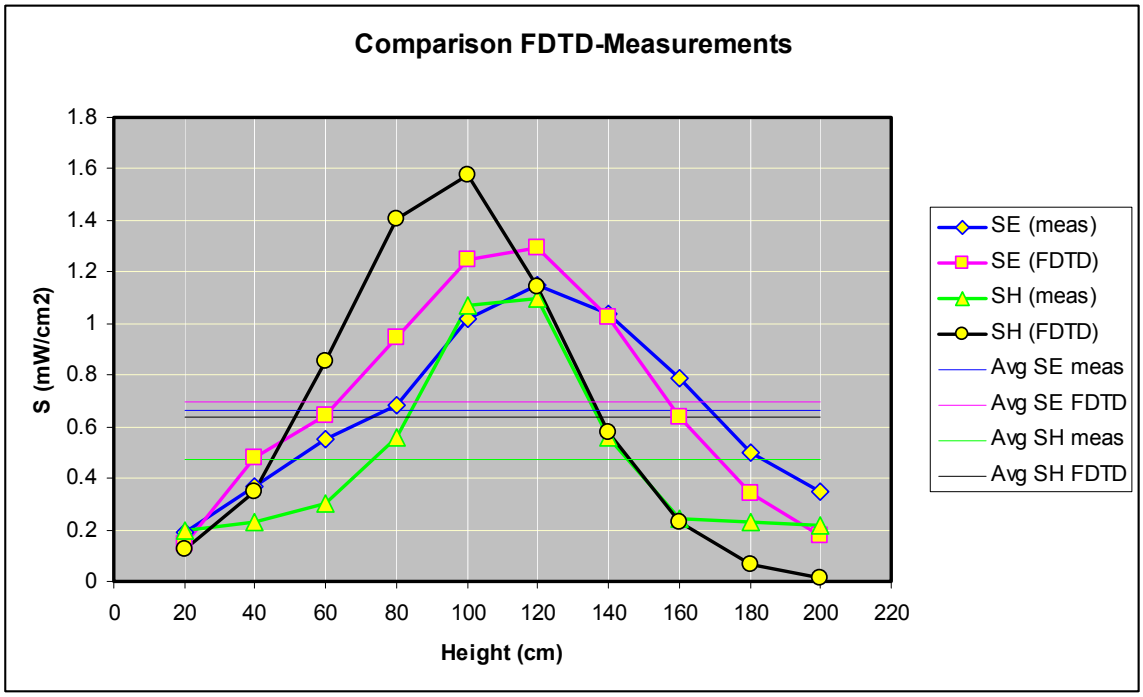

7) Test device positioning

a) A description of the device test positions used in the SAR computations is provided in the SAR report.

b) Illustrations showing the separation distances between the test device and the phantom for the tested configurations are provided in the SAR report.

8) Steady state termination procedures

a) The criteria used to determine that sinusoidal steady-state conditions have been reached throughout the computational domain for terminating the computations are based on the monitoring of field points to make sure they converge. For at least one passenger and one bystander exposure condition, we placed one "field sensor" near the antenna, others between the body and the domain boundary at different locations, and one inside the head of the model. In all simulations, isotropic E-field sensors were placed at opposite corners of the computational domain. We used isotropic E and H field "sensors", meaning

that all three components of the fields are monitored at these points. The following figures show an example of the time waveforms at the field point sensors in the in two opposite points in the computational domain. We selected points near the lowest and highest grid index points. They are shown together in the figure. The highest field levels are observed for the higher index point, as it is closer to the antenna. In all cases, the field reaches the steady-state after a few cycles.

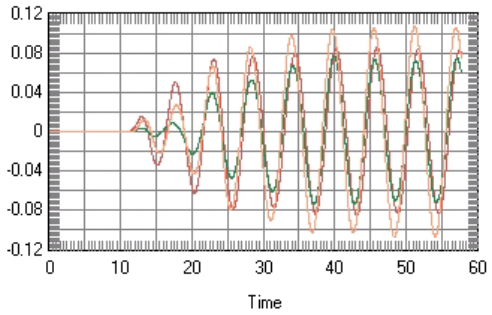

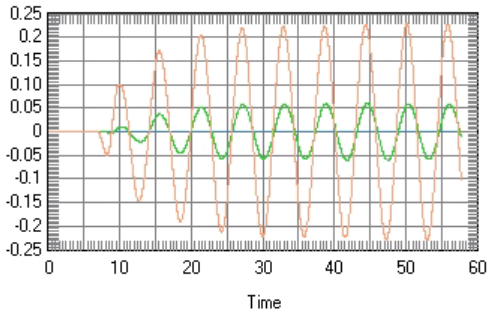

b) 6000 time steps were used, with a time step approximately equal to 10 *ps* (meeting the Courant criterion), which corresponds to 10 wave periods at 149 MHz.

c) The XFDTD™ algorithm determines the field phasors by using the so-called "two-equations two-unknowns" method. Details of the algorithm are explained in [7].

9) Computing peak SAR from field components

a) The twelve E-field phasors at the edges of each Yee voxel are combined to yield the SAR associated to that voxel. In particular, the average is performed on the SAR values computed at the 12 edges of each voxel. Notice that in XFDTD™ the dielectric tissue properties are assigned to the voxel edges, thereby allowing said averaging procedure.

b) The IEEE Standards Coordinating Committee 34, Sub-Committee 2 draft standard P1529 (June 2000) discusses several algorithms for volumetric SAR averaging. It states that "It is observed that while the 12 components algorithm is the most appropriate from the mathematical point of view, the differences in 1g SAR calculated with either the 12 or 6 component methods are negligible for practical mesh resolutions (below 5mm). On the other hand, it is shown that the 3 components approach may lead to significant errors." XFDTD™ employs the 12-component method, which is the one recommended in the draft standard, thus providing the best achievable accuracy.

10) One-gram averaged SAR procedures

a) XFDTD™ computes the Specific Absorption Rate (SAR) in each complete cell containing lossy dielectric material and with a non-zero material density. To be considered a complete cell, the twelve cell edges must belong to lossy dielectric materials. The averaging calculation uses an interpolation scheme for finding the averages. Cubical spaces centered on a cell are formed and the mass and average SAR of the sample cubes are found. The size of the sample cubes increases until the total mass of the enclosed exceeds either 1 or 10 grams. The mass and average SAR value of each cube is saved and used to interpolate the average SAR values at either 1 or 10 grams. The interpolation is performed using two methods (polynomial fit and rational function fit) and the one with the lowest error is chosen. The sample cube must meet some conditions to be considered valid. The cube may contain some non-tissue

cells, but some checks are performed on the distribution of the non-tissue cells. A valid cube will not contain an entire side or corner of non-tissue cells.

b) The sample cube increases in odd-numbered steps (1x1x1, 3x3x3, 5x5x5, etc) to remain centered on the desired cell. Since the visible human model employed herein has 5 mm resolution, the one-gram SAR is computed by averaging first over 1x1x1 voxels, corresponding to 0.125 cm^3 (not enough yet), and then over a 3x3x3 voxel cube, corresponding to about 3.4 cm^3, which is enough to include 1-g, and finally over a 5x5x5 voxel cube, corresponding to about 15.6 cm^3, which includes 10-g. The 1-g average SAR is computed by interpolating these three data points. This procedure is repeated in the surroundings of each voxel that is constituted by lossy materials, so as to determine the 1-g and/or 10-g SAR distributions.

c) As mentioned at points 10(a) and 10(b), the 1- gram average SAR is determined by interpolating the average SAR for the 1x1x1 , 3x3x3, and the 5x5x5 data points, corresponding to 0.125 cm^3, 3.4 cm^3, and 15.6 cm^3, respectively. Because the interpolation is carried out across three data points, the error introduced should be negligible because the interpolating curve crosses exactly the data points.

11) Total computational uncertainty – We derived an estimate for the uncertainty of FDTD methods in evaluating SAR by referring to [6]. In Fig. 7 in [6] it is shown that the deviation between SAR estimates using the XFDTD™ code and those measured with a compliance system are typically within 10% when the probe is away from the phantom surface so that boundary effects are negligible. In that example, the simulated SAR always exceeds the measured SAR.

As discussed in 6(a), a conservative bias has been introduced in the model so as to reduce concerns regarding the computational uncertainty related to the car modeling, antenna modeling, and phantom modeling. The results of the comparison between measurements and simulations presented in 6(a) suggest that the present model produces an overestimate of the exposure between 4% and 36%. Such a conservative bias should eliminate the need for including uncertainty considerations in the SAR assessment.

12) Test results for determining SAR compliance

a) Illustrations showing the SAR distribution of dominant peak locations produced by the test transmitter, with respect to the phantom and test device, are provided in the SAR report.

b) The input impedance and the total power radiated under the impedance match conditions that occur at the test frequency are provided by XFDTD™. XFDTD™ computes the input impedance by following the method outlined in [8], which consists in performing the integration of the steady-state magnetic field around the feed point edge to compute the steady-state feed point current (*I*), which is then used to divide the feed-gap steady-state voltage (*V*). The net *rms* radiated power is computed as

$$P_{XFDTD} = \frac{1}{2}\mathrm{Re}\left\{VI^*\right\}$$

Both the input impedance and the net rms radiated power are provided by XFDTD™ at the end of each individual simulation.

We normalize the SAR to such a power, thereby obtaining SAR per radiated Watt (*normalized SAR*) values for the whole body and the 1-g SAR. Finally, we multiply such normalized SAR values times the max power rating of the device under test. In this way, we obtain the exposure metrics for 100% talk-

time, i.e., without applying source-based time averaging.

c) For mobile radios, 50% source-based time averaging is applied by multiplying the SAR values determined at point 12(b) times a 0.5 factor.

REFERENCES

[1] K. S. Yee, "Numerical Solution of Initial Boundary Value Problems Involving Maxwell's Equations in Isotropic Media," *IEEE Transactions on Antennas and Propagation*, vol. 14, no. 3, 302-307, March 1966.

[2] Z. P. Liao, H. L. Wong, G. P. Yang, and Y. F. Yuan, "A transmitting boundary for transient wave analysis," Scientia Sinica, vol. 28, no. 10, pp 1063-1076, Oct. 1984.

[3] Validation exercise: Mie sphere. Remcom Inc. (enclosed PDF)

Remcom.pdf

[4] NEC-Win PRO ™ v 1.1, Nittany Scientific, Inc., Riverton, UT.

[5] C. M. Collins and M. B. Smith, "Calculations of B1 distribution, SNR, and SAR for a surface coil against an anatomically-accurate human body model," *Magn. Reson. Med*., 45:692-699, 2001. (enclosed TIF)

Collins & Smith.pdf

[6] Martin Siegbahn and Christer Törnevik, "Measurements and FDTD Computations of the IEEE SCC 34 Spherical Bowl and Dipole Antenna," Report to the IEEE Standards Coordinating Committee 34, Sub-Committee 2, 1998. (enclosed PDF)

Ericsson.pdf

[7] C. M. Furse and O. P. Gandhi, "Calculation of electric fields and currents induced in a millimeter-resolution human model at 60 Hz using the FDTD method with a novel time-to-frequency-domain conversion**,"** Antennas and Propagation Society International Symposium, 1996. (enclosed PDF)

Furse & Gandhi.pdf

[8] *The Finite Difference Time Domain Method for Electromagnetics*, Chapter 14.2, by K. S. Kunz and R. J. Luebbers, CRC Press, Boca Raton, Florida, 1993.